Geophys. J. Int. (2007) **169,** 1089–1102 doi: 10.1111/j.1365-246X.2007.03317.x

Seismic tomographic imaging of *P*- and *S*-waves velocity perturbations in the upper mantle beneath Iran

Alireza Alinaghi,[1,2] Ivan Koulakov[3,4] and Hans Thybo[1]

[1] *Geological Institute, University of Copenhagen, Denmark. E-mail: ali@geol.ku.dk*
[2] *International Institute of Earthquake Engineering (IIEES), Tehran, Iran*
[3] *GeoForschungsZentrum, Potsdam, Germany*
[4] *Institute of Geology SB RAS, Novosibirsk, Russia*

Accepted 2006 November 29. Received 2006 November 29; in original form 2006 January 27

SUMMARY

The inverse tomography method has been used to study the *P*- and *S*-waves velocity structure of the crust and upper mantle underneath Iran. The method, based on the principle of source–receiver reciprocity, allows for tomographic studies of regions with sparse distribution of seismic stations if the region has sufficient seismicity. The arrival times of body waves from earthquakes in the study area as reported in the ISC catalogue (1964–1996) at all available epicentral distances are used for calculation of residual arrival times. Prior to inversion we have relocated hypocentres based on a 1-D spherical earth's model taking into account variable crustal thickness and surface topography. During the inversion seismic sources are further relocated simultaneously with the calculation of velocity perturbations. With a series of synthetic tests we demonstrate the power of the algorithm and the data to reconstruct introduced anomalies using the ray paths of the real data set and taking into account the measurement errors and outliers. The velocity anomalies show that the crust and upper mantle beneath the Iranian Plateau comprises a low velocity domain between the Arabian Plate and the Caspian Block. This is in agreement with global tomographic models, and also tectonic models, in which active Iranian plateau is trapped between the stable Turan plate in the north and the Arabian shield in the south. Our results show clear evidence of the mainly aseismic subduction of the oceanic crust of the Oman Sea underneath the Iranian Plateau. However, along the Zagros suture zone, the subduction pattern is more complex than at Makran where the collision of the two plates is highly seismic.

Key words: body waves, Iranian plateau, seismic tomography, upper mantle, velocity perturbations.

INTRODUCTION

The high seismicity and complex tectonic structure of Iran provides a unique opportunity for tomographic investigations of the crust and upper mantle. In the absence of densely distributed seismic stations with accessible data, traditional tomographic methods cannot address this task. However, high seismicity and the availability of phase data reported by global seismic networks enables us to map velocity anomalies using Inverse Tomography (Koulakov 1998; Koulakov *et al.* 2002; Koulakov & Sobolev 2006). The method, which relies on the concept of reciprocity of source–receiver pairs, uses the earthquakes in the study area to calculate velocity perturbations while it simultaneously relocates the sources. The outcome of this approach is a model of the velocity structure as well as improved location of hypocentres in the study region.

Geological and tectonic setting

The current geological and tectonic structure of Iran is the result of the ongoing northward convergence of the Arabian Plate towards Eurasia. The main phase of collision began in the Miocene (Dewey *et al.* 1986). It has trapped Central Iran between the Arabian shield in the south and the Turan Plate in the north and has resulted in the formation of the Iranian plateau, widespread deformation, mountain building and seismicity.

The resulting deformation involves intracontinental shortening and widespread seismicity, except along the southeastern margin of Iran (Makran) where the Oman oceanic lithosphere subducts northwards under southeast Iran (Fig. 1). Within Iran, most of the deformation is assumed to be accommodated in the major mountain belts (Zagros and Alborz) and along large strike-slip faults that surround the blocks (the Central Iranian Desert, the Lut Block and the southern Caspian Sea). These blocks show moderate relief and sparse low seismicity (Jackson & McKenzie 1984; Berberian & Yeats 1999) (Fig. 1).

DATA

The input data consists of the arrival times of *P* and *S* waves from earthquakes in the study area (Fig. 1) as reported by the worldwide

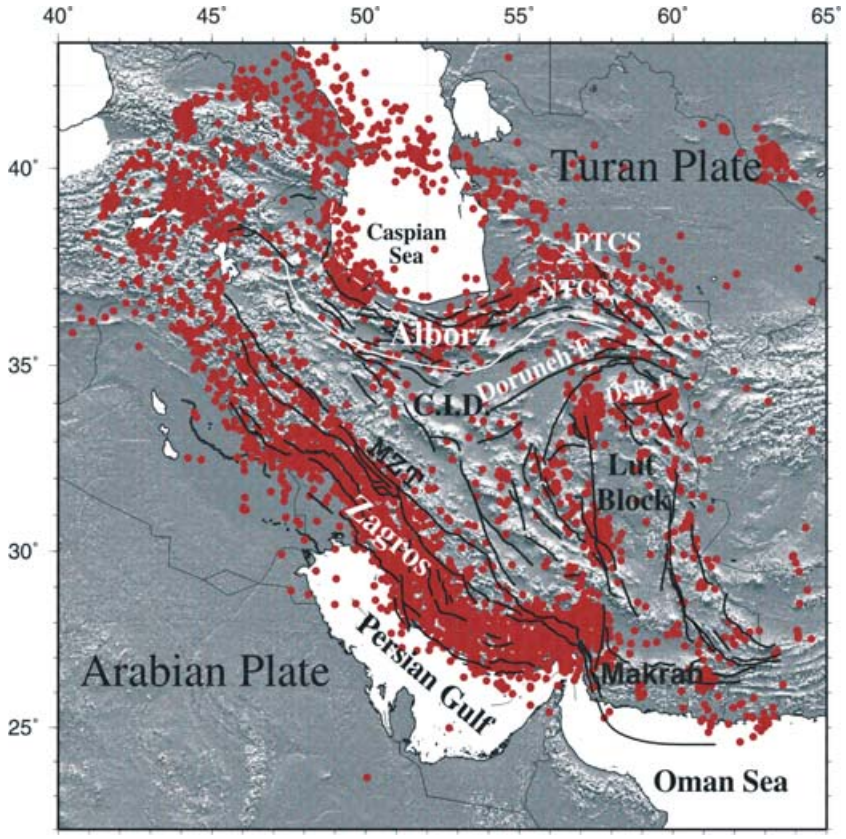

Figure 1. Map of the study area showing Iran and the neighbouring Arabian and Turan plates together with the main structural units: Alborz and Zagros mountain ranges, Lut and Capian blocks and Central Iran microplate (Takin 1972) which are surrounded by major active faults such as Doruneh and Dashte-Bayaz (D.B.F). The boundary between the Zagros mountains and the Central Iranian Desert (C.I.D.) is delineated by Main Zagros Thrust (MZT). Its continuation in the Oman Sea represents the subduction at Makran. Also shown are Palaeo-Thetys (PTCS) and Neo-Thetys (NTCS) and Dorouneh fault. The seismicity shown by red circles is from the ISC bulletins (1964–1996). Vertical and horizontal axis annotations are degrees of north and east geographical latitudes and longitudes, respectively.

seismological stations (Fig. 2) to the ISC for the period of 1964–1996 (ISC 2001). In total we selected 2852 earthquakes in the study region from which 242 664 *P* and 23 207 *S* arrival times are reported by 2081 stations (Fig. 2) of the worldwide network were used. In addition 3856 *pP* and 341 *sS* depth phases were used for constraining the depth of the corresponding sources. A major part of the data set is the arrival times reported by stations in Europe, clearly inferred from the azimuthal distribution of the rays (Fig. 3). The majority of the readings correspond to epicentral distances between 10° and 60° (Fig. 3). Short distance rays (up to 10° of epicentral distance) are chiefly used for source relocation, whereas the teleseismic rays are considered to be the main source of information on deep velocity structure.

METHODOLOGY

Here, we briefly describe the methodology which is discussed in detail by Koulakov & Sobolev (2006).

Prior to inverting the arrival time residuals for simultaneous determination of velocity perturbations and hypocentres parameters, we relocate the hypocentres and recompute the arrival time residuals based on ak135 global velocity model.

Pre-processing of the arrival times for the inversion was performed in two stages. In the first stage *P*- and *S*-waves arrival time residuals with respect to the JB model (Jeffreys & Bullen 1940) in the ISC catalogue were replaced by residuals computed on the basis of ak135 model (Kennett *et al.* 1995). Standard corrections such as those for elevation of the stations and earth ellipticity (Dziewonski & Gilbert 1976) are followed by corrections for variable Moho depths. Moho depths at the piercing points for each source–receiver pair are derived from a model of the crust with a resolution of $1^\circ \times 1^\circ$ (Fig. 4), which is available for most parts of Eurasia and is a compilation of a number of models (http//mahi.uscd.edu/Gabi/rem.html, Laske 2004, personal communication, 2004). For sources and receivers not covered by the high resolution model we use a model of $2^\circ \times 2^\circ$ resolution from Bassin *et al.* (2000).

In the second stage of the processing, hypocentres were redetermined and events with unreliable locations were discarded. Absolute relocation of the earthquakes was done by minimizing the value of a function describing the time residuals first by searching in a regular grid constructed around the preliminary location of the sources (here, ISC location) and then further constraining the location by use of a gradient descending method (Koulakov & Sobolev 2006). During this process the outlier traveltime residuals were identified and sorted out. The outliers are defined as residuals with standard deviations of over 4 s. They constitute 10–15 per cent of data set. The relative relocation of events in clusters was then performed using a double difference method (Waldhauser & Ellsworth 2000) through which a linear system of equations for all combinations of source–receiver pairs in clusters with predefined dimensions are constructed and solved by an iterative LSQR method (van der Sluis & van der Vorst 1987). The static station corrections were

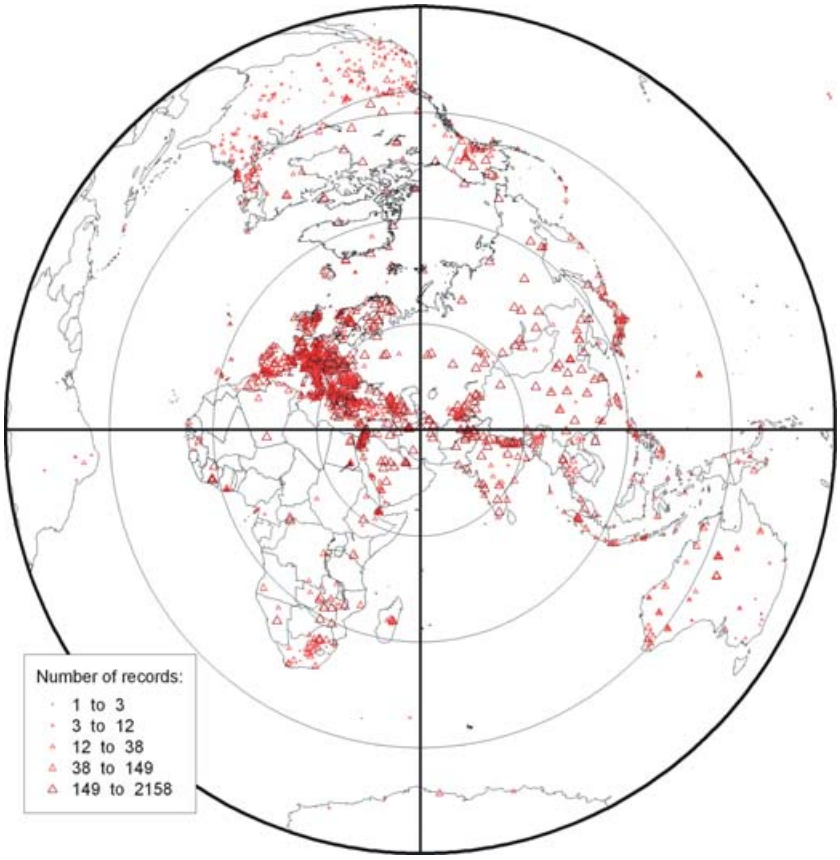

Figure 2. Distribution of the 2081 seismic stations that contributed to the data set used in this study. The size of the triangles reflects the number of events reported by each station. Each circle indicates 30° of epcientral distance. The centre of the figure represents the study region (Iran).

not removed although they were determined simultaneously with hypocentres.

The expected lateral velocity variations are assumed to have amplitudes less than some percentage of the reference velocity and dimensions larger than the Fresnel volume at crustal and upper-mantle depths. The Fresnel zone is estimated to be about 10 km at crustal depths and increases with depth to not above 50 km in the upper mantle. Therefore, the 3-D ray paths from relocated hypocentres to the recording stations are approximated by ray paths in the 1-D reference earth model (ak135, Kennett *et al.* 1995), with the Moho set at 40 km depth as the average crustal thickness in Iran. Ray misplacement and the resulting error in velocity perturbations are insignificant, as we have limited our depth of investigation to about 700 km below the surface which is enough to observe the interaction of tectonic features at upper-mantle depths.

Parametrization and inversion

The velocity field is parametrized by an irregular grid of non-overlapping hexahedra with nodes placed on 16 horizontal planes at depths of 50, 100, 150, 220, 290, 360, 430, 500, 570, 640, 710 and 800 km. On each plane, nodes are distributed along parallel lines with spacing proportional to the ray density (Fig. 5). The nodes on each level are interconnected to form trapezoids. The vertices of trapezoids from adjacent depth levels connect to form a grid of hexahedral cells. Thus, each point in the parametrized study volume is located inside one hexahedron and influenced by eight velocity nodes.

The first derivative matrix which reflects the effect of velocity variations on the traveltime of the rays is composed of two elements for the *P*- and *S*-waves velocity perturbations, four elements for the hypocentres and two elements for station corrections.

An additional matrix block is constructed for smoothing the results, with coefficients for velocity perturbations, source parameters and station corrections. An extra block of the matrix contains arrival times as reported by the stations in the area from teleseismic earthquakes. This is a modification to the inversion scheme presented by Koulakov & Sobolev (2006) and, therefore, the matrix includes both inverse and traditional elements.

The resulting matrix is inverted using the LSQR method (Paige & Saunders 1982; van der Sluis & van der Vorst 1987) for simultaneous determination of *P*- and *S*-waves velocity perturbations, hypocentre parameters and station corrections. By postulating that the inferred velocity anomalies do not bend the original ray paths, basic linearization assumptions are held and a linear inversion is conducted.

Following Koulakov & Sobolev (2006) and Koulakov *et al.* (2002) the whole study area is divided into three smaller overlapping regions. The inversion is performed independently in each region and consequently the results in overlaping areas are averaged. For each block, in order to avoid the bias introduced by alignment of nodes in parallel lines, the final velocity model is calculated as the mean of values in four different orientations of the grids (0°, 45°, 90°

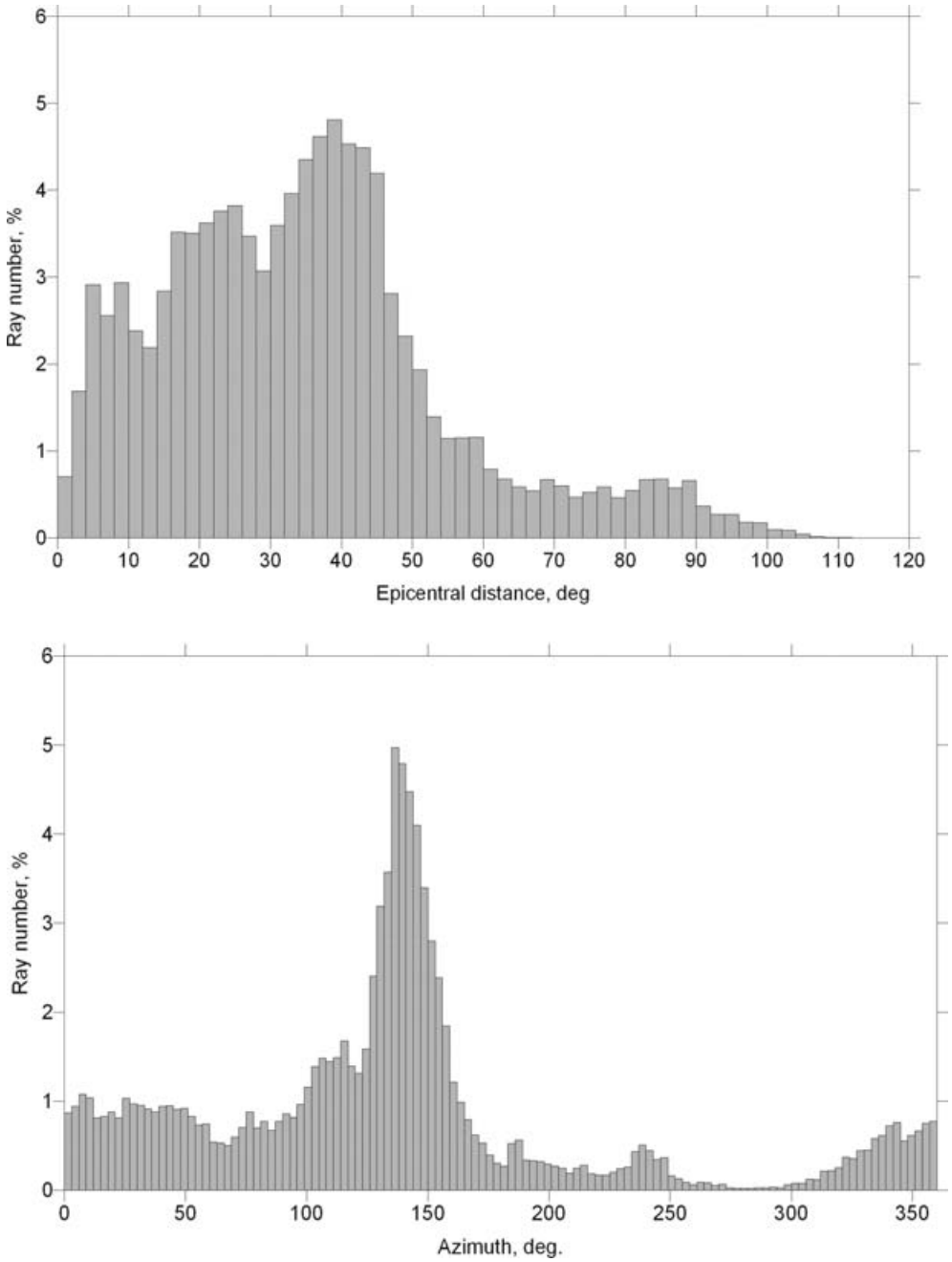

Figure 3. Histograms of data distribution with respect to the epicentral distance (top) and azimuth (bottom).

and 135°). The final model is, therefore, obtained as the average of 12 separate models.

RESULTS

The results of redetermination of the hypocentres are shown in Fig. 6 together with the ISC and EHB (Engdahl *et al.* 1998) locations. Despite insufficient depth phases relocation has been successful in regrouping the events into a number of depth ranges. It is clear that in northern Iran, except for earthquakes across the Caspian Sea most earthquakes are of crustal depth. This is an important indication that along Alborz and its eastern continuation (Kopeh-Dagh) and also at the boundary between the Lut Block and Central Iran (Fig. 1) the earthquakes are related to seismogenic faults located mainly in the upper crust. This pattern changes along the seismic belt across the Caspian Sea, where earthquakes are perceptibly deeper than those in Kopeh-Dagh and in the Caucuses (southeast and northwest of the belt, respectively). Although our relocation has shifted most of the events in Zagros to shallower depths, at its southeastern edge where Zagros abuts the almost aseismic subduction zone of Makran, a concentration of deeper events is observed. The significance and tectonic implications of this observation need further analysis based on local data and waveform analysis.

The results of inversion for the *P*- and *S*-waves velocity anomalies in the study volume are presented in images which resulted from averaging values of three overlapping circular blocks each of a size of 8° in diameter, which jointly cover the whole study region.

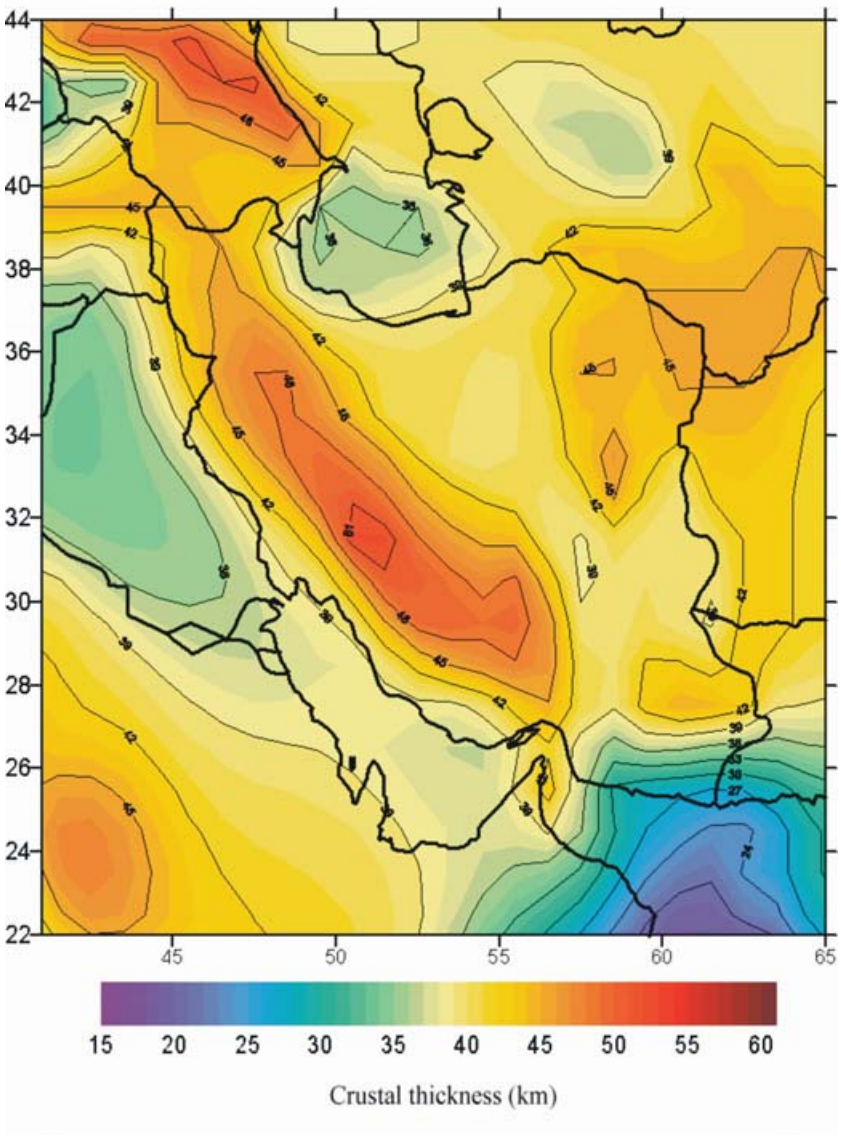

Figure 4. Map of the crustal thickness for Eurasia with $1^\circ \times 1^\circ$ resolution (from http//mahi.uscd.edu/Gabi/rem.html, (Laske, 2004, personal communication, 2004) used in this study for crustal correction. Vertical and horizontal axis annotations are degrees of north and east geographical latitudes and longitudes, respectively.

The velocity anomalies are shown only if the distance to the nearest parametrization node is less than a predefined value of $d_{\max} = 50$ km.

Horizontal sections at different depth levels for both *P*- and *S*-waves velocity anomalies (Fig. 7) show that down to 220 km depth, the tectonically active Iran interior is characterized by low *P*- and *S*-waves velocity anomalies, in contrast to high velocity domains of the Arabian and Eurasian plates to the south and north of the territory. The similarity of the anomaly features in the *P* and *S* horizontal sections is an indication for the conformity of the results. Below the 220 km depth the anomaly signs which leads to complete reversal of pattern below the 410 km discontinuity in the upper mantle so that Central Iran represents a high velocity domain in both *P*- and *S*-waves velocity sections.

In order to assess the success of our pre-processing method in treating the noisy ISC data and to test the effect of our relocation algorithm on the final tomograms, we used the EHB pre-processed global data set of Engdahl *et al.* (1998), which first, utilizes more depth phases than our data set for relocation of sources and secondly, adopts a different approach in identification and discarding the outliers. Using this catalogue we skipped the stage of absolute and relative relocation of earthquakes prior to the inversion. The results presented in horizontal sections (Fig. 8) show striking similarities with the results (Fig. 7), that we obtained by pre-processing the ISC catalogue as described earlier in this paper. The robustness of the results demonstrates that our handling of the noisy ISC data can increase the signal-to-noise ratio to the extent that main structural features are resolvable and stable.

Seven vertical cross-sections (Fig. 9) illustrate how Central Iran is juxtaposed against the Arabian Plate in the south and the Turan Plate in the north. Across the Zagros system, (profiles 1–5) we observe features that indicate both subduction and subsequent collisional stage of convergence between the high velocity Arabian Plate and the low velocity Central Iran. Along Zagros and in particular at

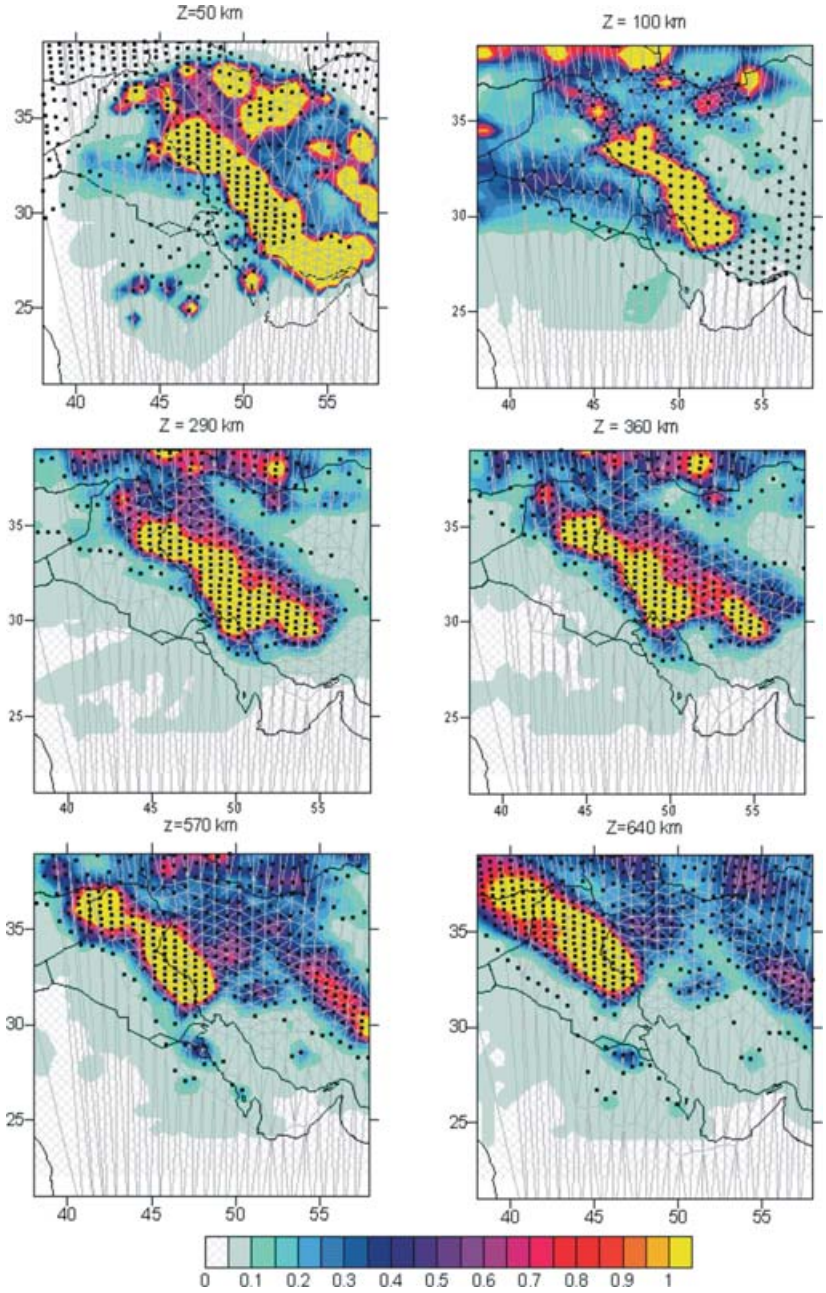

Figure 5. *P*-wave ray density at depth slices from 50 to 640 km for a circular block of 8° (epicentral distance) with 0° grid orientation in the study area, superimposed on grids constructed around nodes (black dots). The colour scale represents normalized values of the ray density with respect to a 50 × 50 km^2 cell at 50 km depth through which 49 014 rays have traversed. Vertical and horizontal axis annotations are degrees of north and east geographical latitudes and longitudes, respectively.

Makran (profiles 6 and 7), structures that indicate subduction are observed. The boundary between Central Iran and Eurasia, along the Alborz mountains appear to be different from the Central Iran to Arabian Shield boundary. This is also reflected by shallow depths of almost all earthquakes in the Alborz system in contrast to more frequently occurring deeper events along Zagros if the patterns of depth distributions rather than absolute depth values are relied on. Besides, an apparently south-dipping high velocity structure in Fig. 9 could be interpreted as a relic of an ancient subduction zone related to the old Tethys. Sensitivity tests as they follow in the next section confirm that these features are real even though exact geometries cannot be imaged in detail.

The results presented above as vertical cross-sections are in good qualitative agreement with the finest global tomography results (0.6° resolution) of the region where two cross-sections across Makran and Caspian Sea were presented (Bijwaard *et al.* 1998).

SENSITIVITY TESTS AND SYNTHETICS

Analysis of the resolution power of the data and algorithm is carried out in a series of sensitivity tests. We have computed the residual traveltimes for synthetic models along the same ray paths as traced for the real data set, and after addition of the noise they are inverted

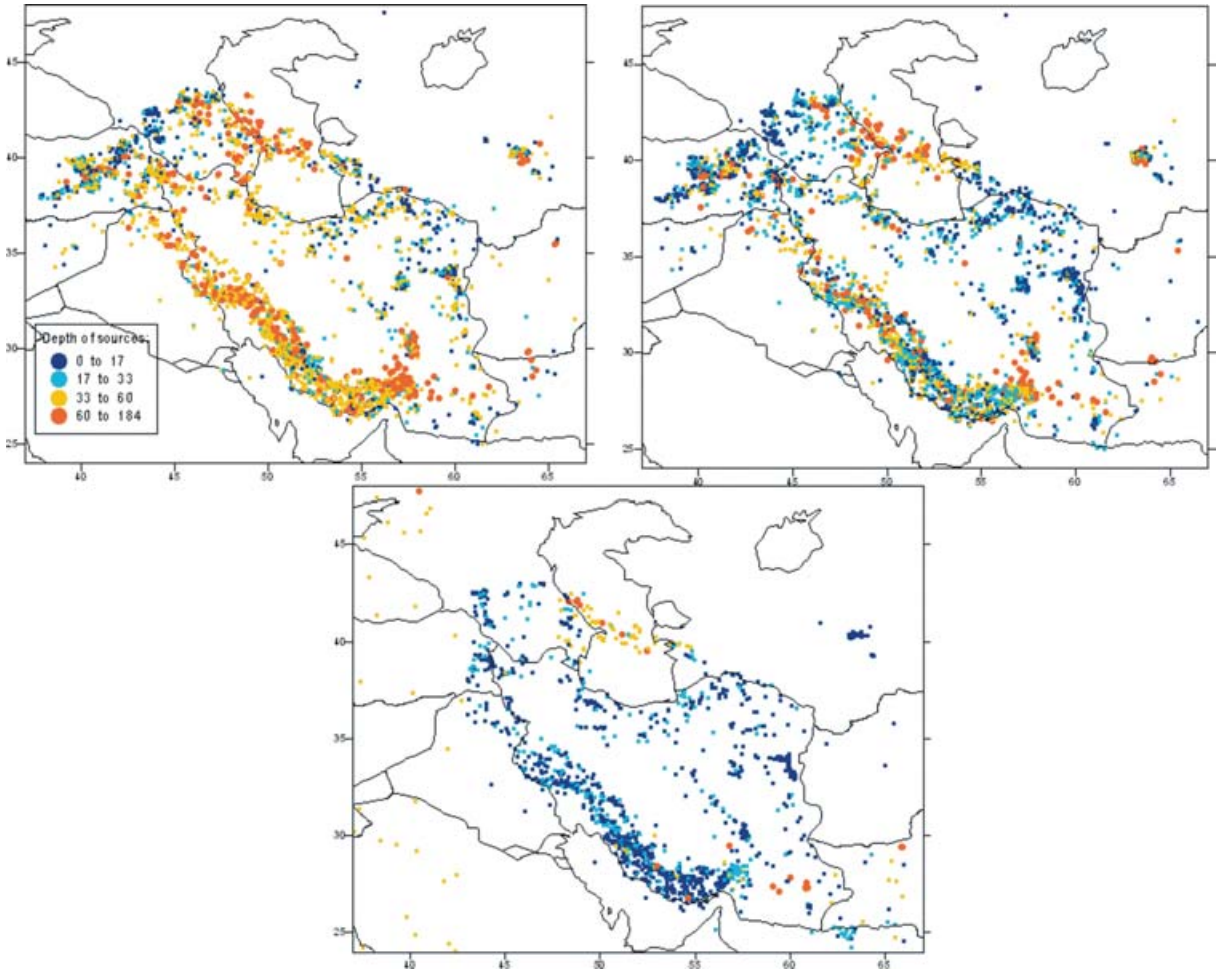

Figure 6. Comparision of the map of the epicentres derived from ISC catalogue (top left) and relocated during this study (top right) with EHB relocations (bottom) as colour coded according to the depths of hypocentres. In spite of insufficient depth phases to appropriately constrain the depths, the relocation algorithm has been successful in regrouping the events as expected from background seismotectonics, where according to ISC locations (left) the distinction is blurred. Vertical and horizontal axis annotations are degrees of north and east geographical latitudes and longitudes, respectively.

in order to test the degree to which we may reconstruct the original synthetic models. This is the approach taken in large tomography studies due to practical problems with computing the resolution matrix for large inverse problems. While we present the results we are aware of the overestimation involved in restoring the anomalies due to neglecting the bending of rays encountering seismic anomalies.

The synthetic times were calculated with delays related to velocity anomalies which are integrated along the ray paths in the reference ak135 velocity model and added to the reference model traveltimes.

Random noise with 1 s standard deviation and a distribution similar to the histogram of the real ISC delays (Fig. 10) was added to delay times. In addition, outlier residual arrival times were introduced with amplitudes of 10 per cent of the noise multiplied by 10, in order to realistically simulate the noisy ISC data (the presence of 10 per cent outliers).

The resulting theoretical arrival times, thus computed, were used as the input data for absolute and relative relocation of the events prior to inversion for velocity perturbations. To achieve unbiased resolution, the synthetic data were inverted with the same parameters as used for the inversion of the actual data.

The first estimation of the resolution was made by the popular checkerboard test in which a 3-D pattern of checkerboard anomalies with alternating signs was used as the synthetic input model (Fig. 11). Through this test we investigate the degree of smearing to which model features are still resolvable. We chose cells of $1^\circ \times 1^\circ$ for the compressional and $2^\circ \times 2^\circ$ for the shear waves taking into account the lower sampling of the study volume by shear waves than by compressional waves. The central part of Iran where the seismicity and consequently the illumination by ray coverage is low, strong smearing is observed. The larger size of the checkerboard cells for the *S* wave synthetics has improved the restoration level while the resolution has decreased. We do not see tangible reduction of restoration level with increasing depths, even though at deeper parts of the upper mantle, larger ray misplacements are expected. Therefore, we conclude that ray misplacement even close to cut-off depth of the study volume is lower than the resolvability of the data and the algorithm. In other words, the linear assumption on the ray tracing does not introduce errors above the resolution limit. We believe that the 1° resolvability of the *P*-wave model which according to this test is an underestimation of the effective resolution is enough to detect subduction features that usually occur on such scales. The smearing is less than 50–100 km in the central parts of the *P* model whereas it is about 100–200 km in the *S*-wave model. At the edge of the models where the ray coverage is low, the smearing

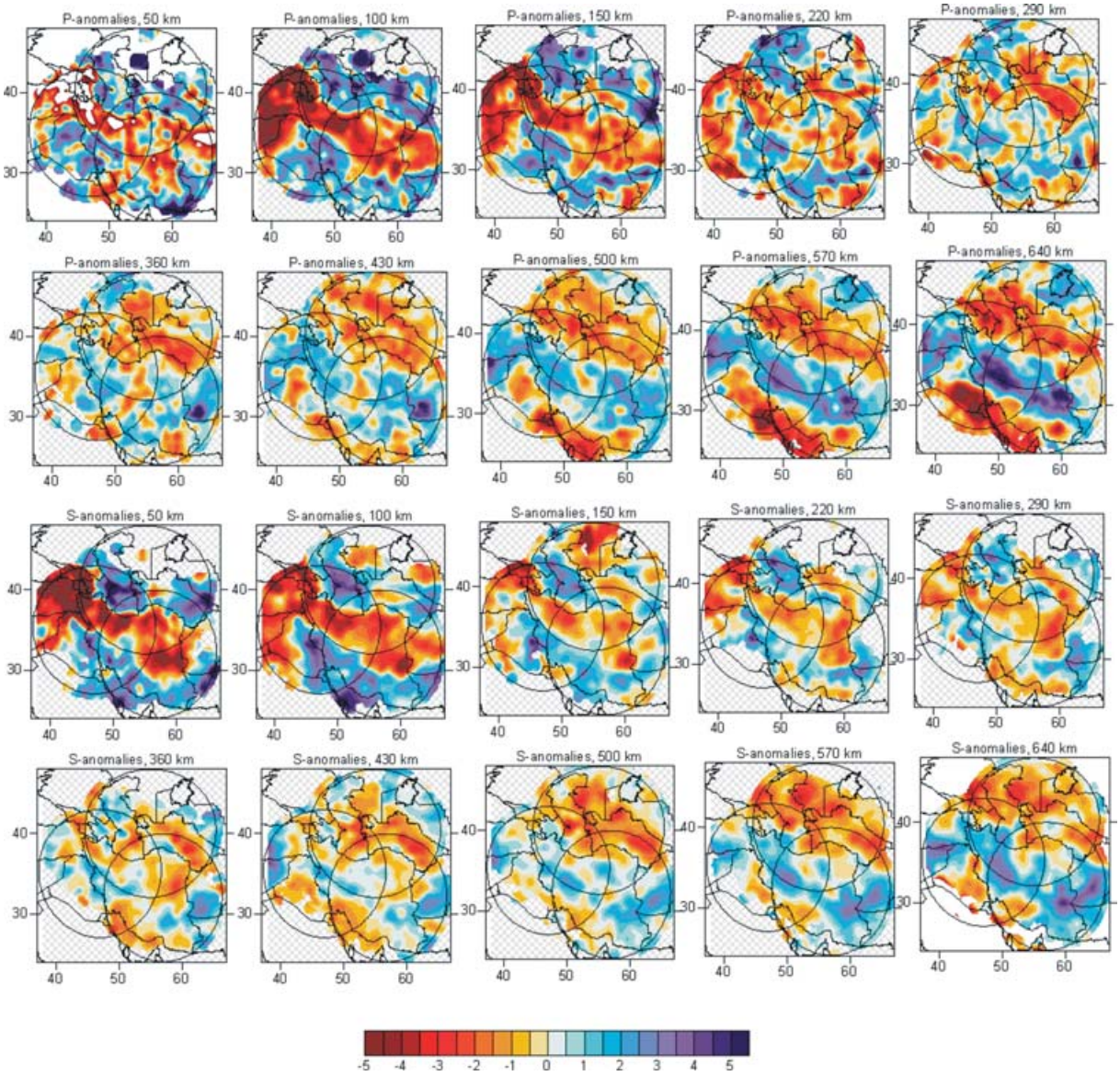

Figure 7. Maps of *P*- and *S*-waves velocity anomalies for Iran and neighbouring regions presented as horizontal sections from depths of 50 to 640 km. Down to the depth of about 220 km, the Iran interior, which is a structural amalgamation of different blocks and microplates, represents a low velocity zone, whereas the underformed Eurasian and Arabian plates to the north and the south, respectively, are high velocity domains. At depths below the 410 km discontinuity in the upper mantle the pattern reverses so that Central Iran in contrast to neighbouring southern and northern territories is a high velocity domain. The colour coded scale represents velocity perturbations in percentage. Vertical and horizontal axis annotations are degrees of north and east geographical latitudes and longitudes, respectively.

approaches 500 km. As expected, smearing and smoothing of the anomalies reduce the amplitudes of the anomalies by distributing the delays over wider zones than in the input model.

The second synthetic test represents a relatively realistic situation where the initial model includes subducting slabs penetrating into the upper mantle, detached slabs and low velocity features in the crust and upper mantle (Fig. 12). Noise with an average rms value of 1.00 s and also, outliers, which constitute 10 per cent of residuals have been added to the input data. Most of the outliers were rejected during the absolute relocation such that the average noise level of the considered residuals due to velocity anomalies was in fact only 0.44 s. This relatively small value may be explained by deep penetration of the synthetic rays. The crustal rays which constitute a significant part of the data set, do not pass through these upper-mantle anomalies and, therefore, have zero values of the residuals. This value of the noise (random noise and outliers) is larger than what is expected from the actual data. Indeed, the variance reduction of the data in this test (15 per cent) is significantly lower than what we observe in the real data (41 per cent).

The inversion which follows the step of absolute and relative relocation of hypocentres has successfully managed to reconstruct the original features especially well in the *P*-wave sections where the ray coverage and amount of data are significantly larger than for the *S* waves. Smearing and deterioration of resolution with increasing depth, as observed in both *P*- and *S*-waves sections, can be attributed to ray misplacements which becomes more severe approaching the cut-off depth of the study volume. This test shows that even with the exaggerated level of the noise, the main patterns are reconstructed

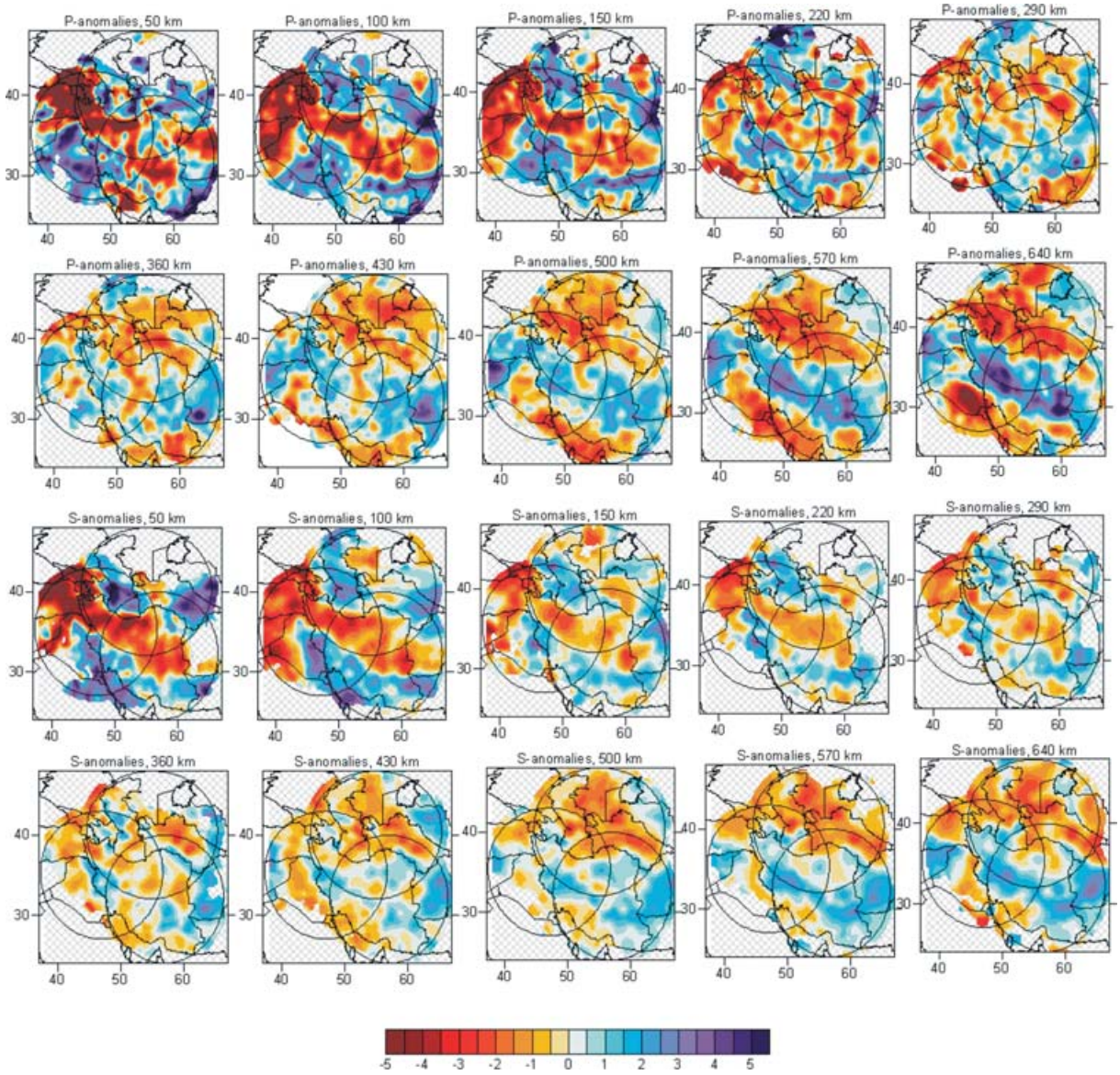

Figure 8. The same as Fig. 7 but based on the EHB earthquake catalogue (Engdahl *et al.* 1998) instead of the pre-processed ISC earthquake catalogue as the input data. All other parameters were held constant for comparing the results. The main features seem to be stable in the two sets of the results. The colour coded scale represents velocity perturbations in percentage. Vertical and horizontal axis annotations are degrees of north and east geographical latitudes and longitudes, respectively.

correctly although stronger smearing of the resulting anomalies is observed at depth. Hence, the necessary relocation seems to have a significant effect on the results. In this synthetic case, the relocation of the sources tends to decrease the resolution. In the real data case, we expect that the simultaneous relocation and inversion for model parameters will increase the obtainable resolution.

Both synthetic tests have shown that the resolution is mainly controlled by the geometry of source and receivers and less by the noise and uncertainties in the traveltime readings.

DISCUSSION

The use of 1-D ray tracer is economically viable for huge matrices like in our case. However, it can cause mislocation of rays especially at lower mantle depths. In order to alleviate this spurious effect we set the cut-off depth of our investigation to about 700 km, which is deep enough to map the tectonic features of interest. Besides, numerical modelling (Zhao & Lei 2004) has shown that the mislocation of the *P* ray travelling about 40°, epicentral distance (which roughly corresponds the distance that the bulk of the rays in our data traverse) calculated using a 3-D ray tracer compared to a 1-D ray tracer at the midpoint is less than 50 km at the most. This is lower than the resolution of our findings and, therefore, we do not expect large discrepancies with results obtained using a 3-D ray tracer in our future work. Assuming that the amplitudes of mapped velocity anomalies are within a few percents of the 1-D reference velocity model we have simplified the problem by avoiding consideration of bending of rays and solving the inverse problem non-linearly.

The variable cell size of the parametrized grid provides a means to increase the resolution where the number of crossing ray paths is low and thus high amplitude artefacts related to poor sampling are reduced. To reduce similar high amplitude spurious anomalies

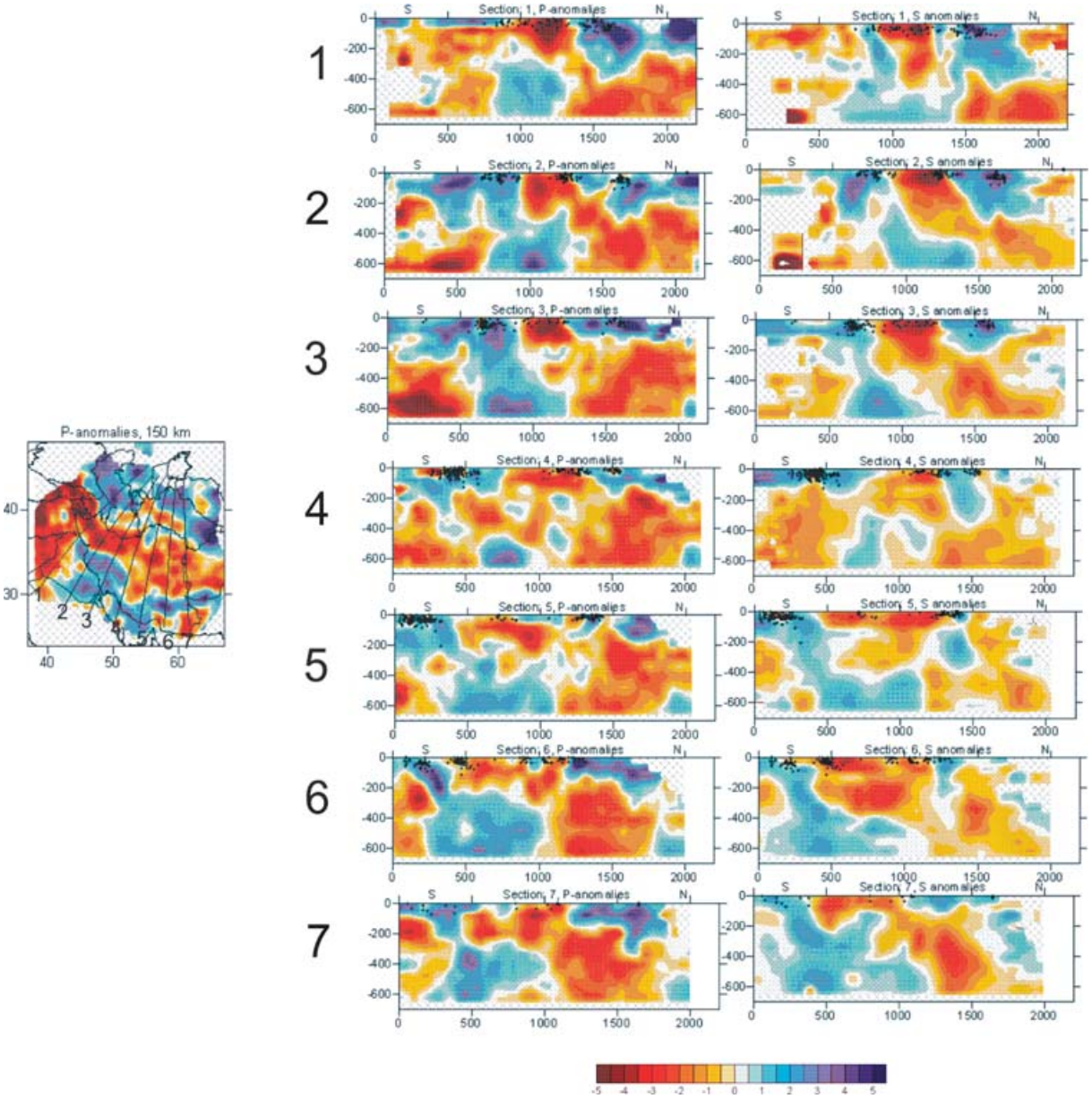

Figure 9. Vertical cross-sections showing the results of inversion for *P* (left panels) and *S* (right panels) velocity anomalies across seven profiles as indicated on the small map (left) and depicted from top to bottom. The north dipping high velocity structures observed along profile 3 (across the western part of the Zagros) and profile 6 (the Makran region) are interpreted as images of subduction of the Arabian Plate under Iran whereas its absence is interpreted as evidence for continental collision. The colour coded scale represents velocity perturbations in percentage. Dots represent the hypocentres of the earthquakes. The unit of the vertical and horizontal axes is km.

at the border of the circular blocks, we have averaged the values of overlapping blocks. While we have attempted to correct for such amplitude artefacts we are aware of the inherent uncertainty involved in recovering the amplitudes of anomalies in traveltime tomography. Therefore, we would rather put the emphasis on the restoration of the shape of the anomalies and not on their amplitude.

The relocation of the hypocentres which is a necessary step, prior to inversion, produced dislocation vectors comparable to those presented by Engdahl *et al.* (1998), even though the outliers were identified and sorted out automatically and depth estimates suffer inaccuracies mainly related to an insufficient number of depth phases or erroneous reporting of them. We have inverted the residuals based on our own relocations and those of Engdahl *et al.* (1998). The results of inversion for *P* and show striking similarities. The reason might lie in the fact that since the inversion is done simultaneously for velocity perturbations and source parameters, the dislocation vectors of hypocentres are of the same order of magnitude (Bijwaard *et al.* 1998) as the formal hypocentre errors determined by Engdahl *et al.* (1998).

Series of resolution tests were presented with emphasis on the upper mantle rather than crustal structures. This emphasis can be explained with respect to poor sampling of the crust by the teleseismic rays. Considering the steep incidence angles it is also expected that an overall vertical averaging of velocity perturbation is observed. Furthermore, at larger depths of the upper mantle the increase of non-geometrical ray effects (Wielandt 1987; Nolet 1992) has led to

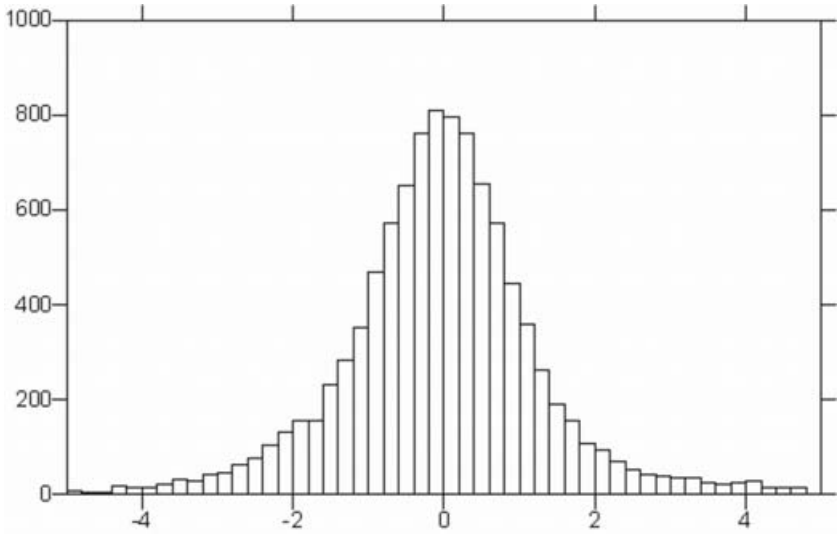

Figure 10. Histogram showing the distribution of the noise simulated after the ISC noise pattern that was added to synthetic arrival times. The vertical axis represents the counts and horizontal axis the measurement error in seconds.

widening of anomalous features such as high velocity subducting slabs. Another extreme case of ray path mislocation is at triplication points where a slight change in the ray take off angle can mean very different ray paths for similar traveltimes (Nolet *et al.* 1994). One approach to avoid this error is to exclude the rays from epicentral distances less than 25°. However, this approach was not adopted due to the obvious disadvantage of discarding rays that give information on shallow structures.

CONCLUSIONS

We have presented seismic tomograms of the crust and the upper mantle of Iran on scales comparable with those of regional tomographic studies. Based on the concept of source–receiver reciprocity, it was shown that in the absence of adequately spaced seismological stations and local phase readings, it is possible to conduct a regional and teleseismic tomography if the study area has sufficient seismicity.

We are aware of the shortcomings of the 1-D forward solver used in this study which might involve ray misplacement and consequently mislocation of seismic anomalies especially at deeper parts of the upper mantle. However, for resolving large anomalies such as those targeted in this study and by holding the realistic assumption that expected velocity perturbations are in the range of a few percents of the 1-D global reference model, we could neglect non-linear effects.

The relocated hypocentres are considered as an improvement to the existing ISC catalogue but since in our procedure reidentification of phases have not been made for redetermination of sources, the location accuracy of 5–10 km claimed by Engdahl *et al.* (1998) that also used more phases for relocation, might have been impaired. The depth estimation yet suffers more from inaccuracies due to the teleseismic nature of most relocations and inadequate depth phases. However, the general pattern presented in this paper has shown the general trends which can be relied on. While the earthquakes in northern Iran appear to be shallow, the events across the Caspian Sea and along the Zagros mountains seem to be deeper. Until better depth estimates are achieved, it is hard to associate clusters of shallow earthquakes in the Zagros system with surface faulting which is responsible for crustal thickening and shortening. Only few earthquakes are located in the Makran region and hence the conclusion is made that the active subduction in the Makran region is mainly aseismic.

The results of inversion for velocity perturbations show that Central Iran, down to a depth of *ca.* 200 km, is a low velocity seismic domain which is bounded by the high velocity Arabian and Eurasian Plates. This is in accordance with expectations from active orogenic belts. Our tomographic results support the idea that the northward movement of the Arabian Plate towards Eurasia has resulted in continental collision along the Zagros mountains but it seems that it is does not appear to involve a simple model. Tomograms also show an active subduction in the Makran region in the southeastern corner of Iran. Features that may be interpreted as active subduction in the Makran region are clearly imaged in both the *P*- and *S*-waves velocity profiles. Our results indicate that the convergence of the Arabian Shield towards Central Iran involves subduction and continental collision, whereas we find only slight evidence of subduction at the boundary of Central Iran with Eurasia in the north.

To assess the reliability of our results and to show the resolution power of the data and algorithm we conducted a series of synthetic tests. Seismic anomalies with various shapes, polarities and locations in the crust and upper mantle were introduced in the study volume, and synthetic arrival times were calculated for the known source–receiver configuration. The synthetic arrival times were then inverted to retrieve model parameters. The synthetics study also included the addition of measurement noise and outliers into the calculated arrival times before inversion. The results showed high seismicity of Iran provides enough ray coverage to resolve the anomalies at upper-mantle depths. The synthetic tests have shown that where the ray coverage is satisfactory such as where the Zagros subduction zone lies, the model features are consistently resolvable for all reasonable choices of inversion parameters. Probably, the high stability of the algorithm is to a large extent achieved by the use of seismic waves at all distance ranges available from local and regional to teleseismic distances.

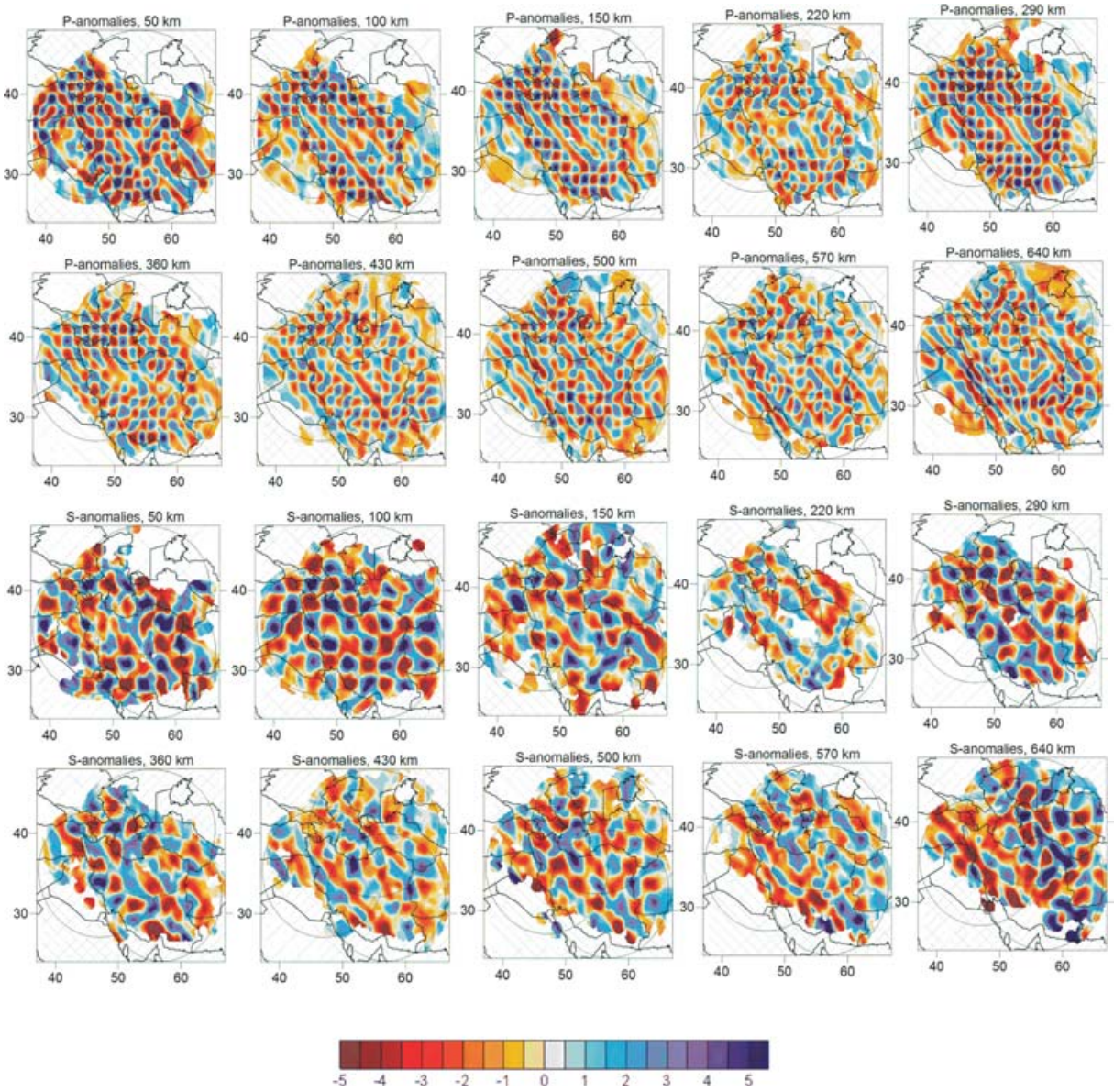

Figure 11. Restoration test of the power of the data and algorithm to resolve a checkerboard pattern of anomalies with cells of about 50 × 50 km^2 for the *P* wave and about 100 × 100 km^2 for the *S* wave. In Iran interior the resolution decreases mainly due to lower number of earthquakes and reduced ray density which results in additional smearing. Vertical and horizontal axis annotations are degrees of north and east geographical latitudes and longitudes, respectively.

ACKNOWLEDGMENTS

AA, IK and HT would like to thank Walter Mooney from USGS for his review of the first draft of the article and his constructive suggestions. AA is obliged to express his utmost gratitude to Edi Kissling for the fruitful discussions during his visit to ETH. Last, but not least, AA, IK and HT thank the Carlsberg Foundation for their generous grant and support to AA, which made this study possible.

REFERENCES

Bassin, C., Laske, G., Masters, G., Bassin, C., Laske, G. & Masters, G., 2000. The current limits of resolution for surface wave tomography in North America, *EOS, Trans. Am. geophys. Un.,* **81,** F897.

Berberian, M. & Yeats, R.S., 1999. Patterns of historical earthquake rupture in the Iranian plateau, *Bull. seism. Soc. Am.,* **89,** 120–139.

Bijwaard, H., Spakman, W. & Engdahl, E.R., 1998. Closing the gap between regional and global travel time tomography, *J. geophys. Res.,* **103,** 30 055–30 078.

Dewey, J.F., Hempton, M.R., Kidd, W.S., SarogClu, F. & Sengor, A.M.C., 1986. Shortening of continental lithosphere: the neotectonics of Eastern Anatolia a young collision zone, in *Collision Tectonics,* **Vol. 19,** pp. 3–36, eds, Coward, M.P. & Ries, A.C., Geol. Soc. Spec. Publ., London.

Dziewonski, A.M. & Gilbert, F., 1976. The effect of small, aspherical perturbations on travel times and a re-examination pf the correction for ellipticity, *J. R. Astr. Soc.,* **44,** 7–17.

Engdahl, E.R., van der Hillst, R.D. & Buland, R.P., 1998. Global teleseismic earthquake relocation with improved travel times and procedures for depth determination, *Bull. seismol. Soc. Am.,* **88,** 722–743.

International Seismological Centre, 2001. Bulletin Disks 1–9 [CD-ROM], Internatl. Seis. Cent., Thatcham, UK.

Jackson, J. & McKenzie, D., 1984. Active tectonics of the Alpine-Himalayan belt between western Turkey and Pakistan, *Geophys. J. R. astr. Soc.,* **77,** 185–264.

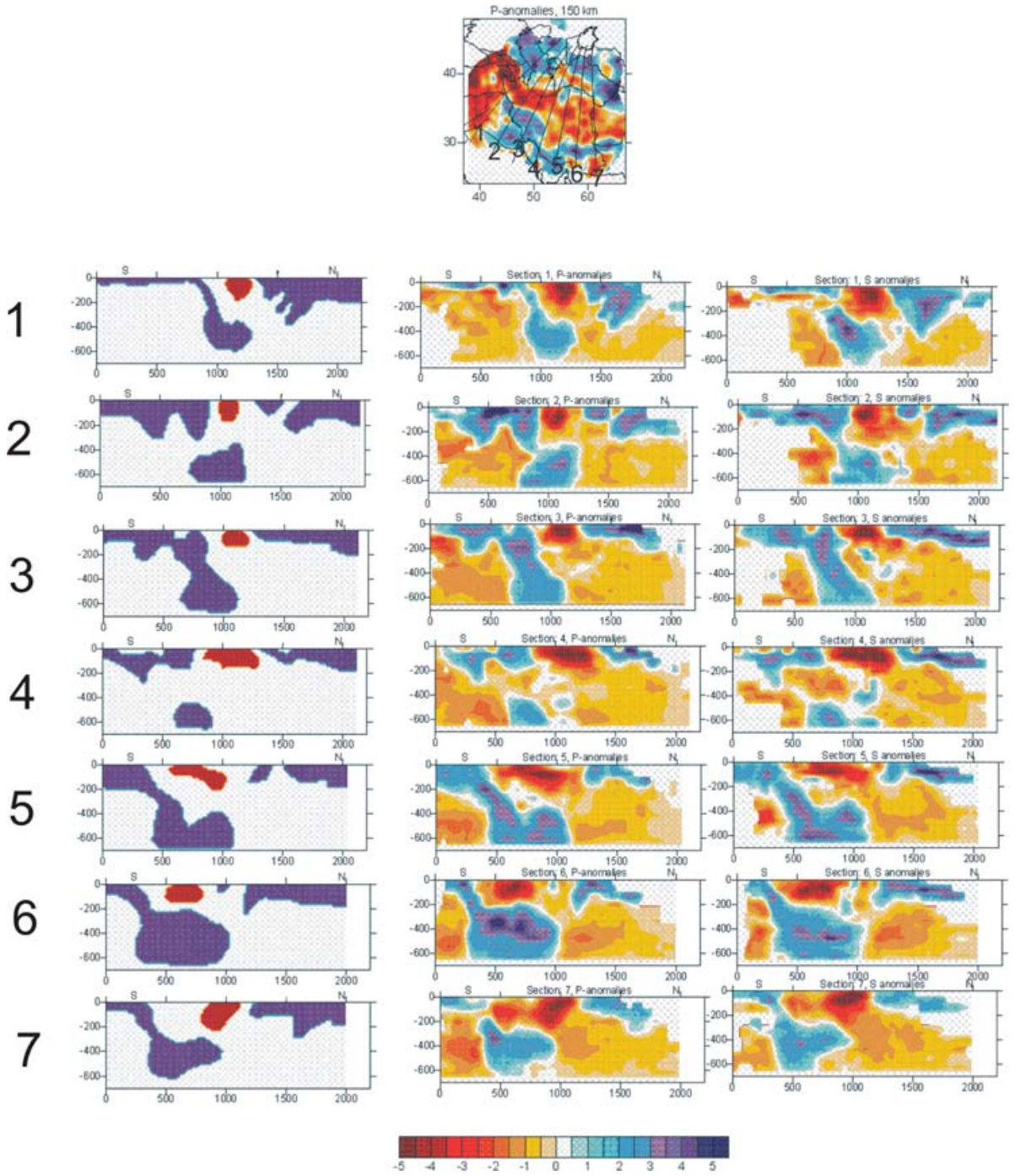

Figure 12. Reconstructions of realistic anomalies in the study area (left column) and the results of inversion for the *P* (middle column) and *S* (right column) waves. Top panel shows the location of cross-sections and lower panels depict the vertical sections along the designated lines on the map. Zagors and the subduction zone in Makran is simulated by a subducting slab of varying shape and flattening part encountering the upper-mantle transition zone. Smearing is more pronounced in *S* wave anomalies mainly due to the smaller amount of *S* readings (only 10 per cent of total readings). However, in both *P* and *S* reconstructions, the subducting slab and geometric shapes are well resolved. The colour coded scale represents velocity perturbations in percentage.

Jeffreys, H. & Bullen, K.E., 1940. Seismological tables, *Brtitish Association for the Advancement of Sciences,* London.

Kennett, B.L.N., Engdahl, E.R. & Buland, R., 1995. Constraints on seismic velocities in the Earth from traveltimes, *Geophys. J. Int.,* **122,** 108–124.

Koulakov, I., 1998. Three-dimensional seismic structure of the upper mantle beneath the central part of the Eurasian continent, *Geophys. J. Int.,* **133,** 467–489.

Koulakov, I. & Sobolev, S., 2006. A tomographic model of Indian lithosphere break-off beneath the Pamir-Hindukush region, *Geophys. J. Int.,* doi:10.1111/j.1365-246X.2005.02841.x

Koulakov, I., Tychkov, S., Bushenkova, N. & Vasilevskiy, A., 2002. Structure and dynamics ovf the upper mantle beneath the Alpine-Himalayan orogenic belt, from teleseismic tomography, *Tectonophysics,* **358,** 77–96.

Nolet, G., 1992. Imaging the deep earth: technical possibilities and theoretical limitations, in *Proceedings of the 25th ESC Symposium Barcelona*

1990, pp. 107–115, Rocca, A. & Mayer-Rosa, D., eds, Servei Geologic de Catalunya, Barcelona, Spain.

Nolet, G., Grand, S.P. & Kennett, B.L.N., 1994. Seismic heterogeneity in the upper mantle, *J. geophys. Res.,* **99,** 23 753–23 766.

Paige, C.C. & Saunders, M.A., 1982. LSQR: An algorithm for sparse linear equations and sparse least squares, *ACM trans. Math. Soft.,* **8,** 43–7.

Takin, M., 1972. Iranian Geology and continental Drift in the Middle East, *Nature,* **235**(5334), pp. 147–150.

van der Sluis, A. & van der Vorst, H.A., 1987. Numerical solution of large, sparse linear algebraic systems arising from tomographic problems, in *Seismic Tomography,* pp. 49–83, ed. Nolet, G., Reidel, Dortrech.

Waldhauser, F. & Ellsworth, W.L., 2000. A double-difference Earthquake location algorithm: method and application to the northern Hayward fault, California, *Bull. seism. Soc. Am.,* **90**(6), 1353–1368.

Wielandt, E., 1987. On the validity of the ray approximation for interpreting delay times, in *Seismic Tomography,* pp. 85–98. ed. Nolet, G., Reidel, Dordrecht.

Zhao, D. & Lei, J., 2004. Seismic ray path variations in a 3D global velocity model, *Phys. Earth planet. Inter.,* **141,** 153–166.